Forbidden $2s_{1/2}$-$1s_{1/2}$ radiative atomic transition

B. Galley and J.-Cl. Dousse
Physics Department, University of Fribourg, CH-1700 Fribourg, Switzerland
(Received 31 March 1994)

The relativistic $K\alpha_3$ ($2s_{1/2}$-$1s_{1/2}$) x-ray transition induced by photoionization was observed in $_{54}$Xe, $_{59}$Pr, $_{64}$Gd, $_{67}$Ho, $_{73}$Ta, and $_{79}$Au. The transitions were measured with a transmission curved-crystal spectrometer. $I(K\alpha_3)/I(K\alpha_1)$ as well as $I(K\alpha_2)/I(K\alpha_1)$ intensity ratios are presented and compared with multiconfiguration Dirac-Fock and Dirac-Hartree-Slater predictions. A good agreement is obtained. No systematic deviation as a function of Z is observed.

PACS number(s): 32.30.Rj, 32.70.Fw, 32.70.Jz, 32.80.Fb

I. INTRODUCTION

In the last several decades, the problem of x-ray emission by atoms has been widely investigated. This is not surprising because x-ray spectroscopy is a powerful tool which provides rich and valuable information about the atomic structure and enables one to check the validity of theoretical models.

In particular, K x-ray lines have been the subject of intensive studies. Regarding the $K\alpha_1$ ($2p_{3/2}\rightarrow 1s_{1/2}$) and $K\alpha_2$ ($2p_{1/2}\rightarrow 1s_{1/2}$) x-ray lines, numerous and consistent data can be found in the literature. Their energies, linewidths and relative intensities are in general well reproduced by theoretical calculations. For the $K\alpha_3$ ($2s_{1/2}\rightarrow 1s_{1/2}$) transition, which is forbidden by the selection rules of both nonrelativistic electric-dipole ($E1$) and electric-quadrupole ($E2$) single-electron transitions, the situation is completely different. Experimental data for magnetic-dipole ($M1$) transitions are scarce and mostly inconsistent. For instance, measured $I(K\alpha_3)/I(K\alpha_1)$ intensity ratios differ strongly from the predicted values by a factor of 0.3–2.1 [1–7]. These discrepancies arise mainly from the poor statistics characterizing most of the measurements and the fitting method used to extract the intensity of the $K\alpha_3$ line. Since the latter appears as a very weak bump superposed on the low energy tail of the diagram $K\alpha_2$ line, its intensity is indeed very sensitive to the fitted shape of the $K\alpha_2$ tail.

The present paper describes the results of high resolution crystal diffractometry measurements of radiative $K\alpha_3$ transitions induced by photoionization in xenon ($Z = 54$), praseodymium ($Z = 59$), gadolinium (Z=64), holmium (Z=67), tantalum (Z=73), and gold (Z=79). To our knowledge the $K\alpha_3$ x-ray lines of xenon (Fig. 1) and praseodymium have never been observed before.

The paper is organized as follows: Sec. II presents the experimental method. The procedure used for the analysis of the data is described and discussed in Sec. III. Measured $I(K\alpha_3)/I(K\alpha_1)$ and $I(K\alpha_2)/I(K\alpha_1)$ intensity ratios as well as experimental $K\alpha_3$ energies are given in Sec. IV where they are compared to other existing experimental results and theoretical predictions (Scofield's Dirac-Hartree-Slater [8] and multiconfigurational Dirac-Fock [9] calculations). Finally, a brief conclusion regarding the $K\alpha_3$ relative yields is drawn in Sec. V.

II. EXPERIMENTAL METHOD

The measurements were performed at the University of Fribourg with a transmission curved crystal spectrometer. A detailed description of a similar instrument installed by our group at the Paul Scherrer Institute (PSI) variable energy cyclotron in Villigen, Switzerland, can be found in Ref. [10], while some experimental features specific to the spectrometer of Fribourg are given in Ref. [11].

For low counting rate type measurements as the one discussed here, the long term stability of the target position and target shape is crucial. For that reason, the spectrometer was operated in the so-called modified DuMond slit geometry. In this geometry, a slit 0.1 mm wide located on the Rowland's circle at a fixed position served as the effective source of radiation. The slit consisted of two juxtaposed lead plates 5 mm thick. 40 mm high and 4 mm wide self-supported metallic targets of natural praseodymium (62 mg/cm^2 thick), gadolinium (78 mg/cm^2), holmium (63 mg/cm^2), tantalum (171 mg/cm^2), and gold (255 mg/cm^2) were used. The targets were placed 1.75 cm behind the slit and tilted at a certain angle to the target-crystal direction. The optimal angle was determined for each target in order to maximize the counting rate. For the xenon measurements a cylindrical cell filled up to 3 bar pressure with 99.99% pure xenon was used. The cell was 3 cm in diameter and 3 cm high with a 11 mg/cm^2 thick kapton cylindrical wall. It has to be noted here that, due to the slit, only a vertical slice with an average thickness of about 0.15 mm contributed to the production of the observed $K\alpha$ x rays and not the complete volume of the cell. The density of the gaseous target was 14.7 mg/cm^3 and the distance between the slit and the axis of the cylindrical cell 2.75 cm.

For the photoionization, we used a Coolidge x-ray tube with a gold anticathode and a nonporous beryllium sheet as window. The tube was connected to a 3-kW high-voltage generator equipped with a dedicated system for

the stabilization of the current and the high voltage of the tube. For the measurements of Xe and Pr, the tube was operated at 85 kV×30 mA, for the Gd and Ho ones at 80 kV×30 mA and for the Ta and Au ones at 95 kV× 30 mA. The distance between the tube and the target was 4.5 cm and the angle between the ionizing radiation beam and the target-crystal direction was 90°.

The (110) planes of a 1 mm thick SiO_2 crystal were used for the diffraction of the x rays. The crystal plate was bent to a radius of curvature of 313 cm and the reflecting area was 26.4 cm^2. The Bragg angles were measured with an optical laser interferometer [12], the accuracy of which varied between 3 and 5 marcsec throughout the angular range (2.1°–5.0°) corresponding to the observed $K\alpha$ spectra.

The full width at half maximum (FWHM) angular resolution Γ_θ of the spectrometer, that depends mainly on the crystal mosaicity and crystal curvature precision and on the slit width was about 9.6 arcsec. The FWHM energy resolution Γ_E is given by

$$\Gamma_E = \cot(\theta) E \Gamma_\theta, \tag{1}$$

where θ is the Bragg angle and E the energy of the diffracted x rays. From this equation one can deduce that the instrumental resolution varied in the presented measurements between approximately 16 eV (Xe) and 87 eV (Au), i.e., matched almost the natural linewidths of the measured transitions (14 eV for Xe and 63 eV for Au).

For the detection of the x rays a Ø5×0.25-in.^{2} NaI(Tl)×2-in. CsI(Tl) phoswich[1] scintillation detector was used. Both NaI and CsI crystals were mounted on the same photomultiplier tube. Because the signals have different rise times, they could be identified by the pulse shape analysis method [13]. In fact, the signals of the rear CsI crystal were used as anticoincident gate pulses for the analog-to-digital converter performing the pulse height analysis of the NaI signals. Most of the Compton events in the front scintillator could thus be suppressed.

All our measurements were carried out in first order of reflection. Each target was measured in two stages: (1) The $K\alpha$ spectrum was first observed on both sides of reflection in order to determine the zero Bragg angle required for the energy calibration of the spectrometer. The $K\alpha$ spectrum measured on the left side of reflection was further used to determine the $K\alpha_1$ and the $K\alpha_2$ line shapes. A precise knowledge of the latter is needed for a correct determination of the yield of the weak $K\alpha_3$ line (see Sec. III). The $K\alpha$ spectrum of xenon is depicted for illustration in Fig. 1.

(2) The angular range corresponding to the energy region of the $K\alpha_3$ line was measured on the left side of reflection in eight successive step-by-step scannings. Each angular scanning consisted of 60 equidistant points. The acquisition time per point was 1000 s. In order to survey the instrumental reproducibility and the stability of the x-ray tube intensity, a short measurement of the $K\alpha_1$ line was performed between each scanning. The aim of these $K\alpha_1$ measurements was to normalize *a posteriori* the $K\alpha_3$ line intensity and to adjust the energy scale of each scanning with respect to the first one. In fact, the analysis showed that the fluctuations of the $K\alpha_1$ line intensity were for all measurements smaller than 1.3 %. Similarly, the standard deviation of the average energy of the $K\alpha_1$ centroids was found to be, in the worst case, less than 3 eV. No correction was therefore performed and for each target the eight scannings were simply added to get the $K\alpha_3$ spectrum. Such $K\alpha_3$ sum spectra are shown in Figs. 1 (inset), 2, and 3.

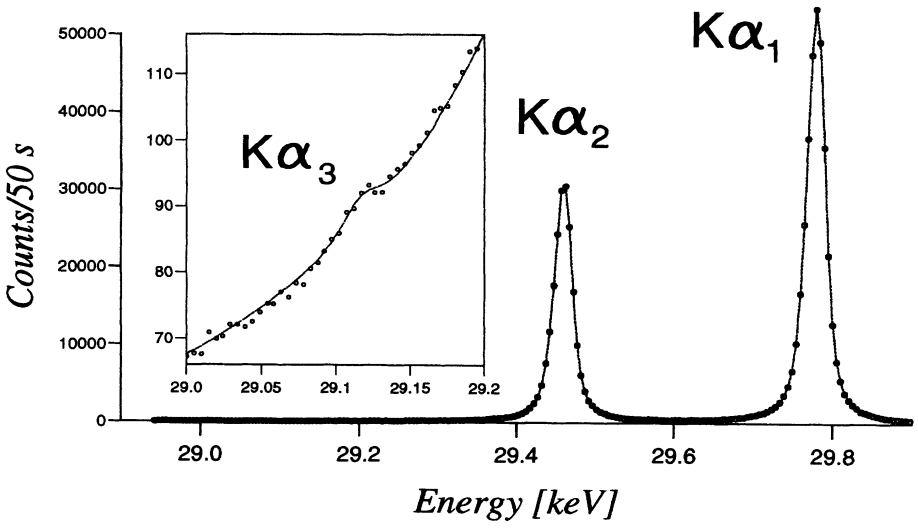

FIG. 1. $_{54}$Xe crystal spectrometer spectrum of $K\alpha$ x rays induced by photoionization. The dots correspond to the experimental points and the curves to the fit. The weak bump shown in the inset corresponds to the $K\alpha_3$ x-ray line. The vertical scale of the $K\alpha_3$ spectrum was normalized to an acquisition time of 50 s (real time was 8000 s).

[1]Phoswich is a trademark for a two-component scintillation detector developed by The Harshaw Chemical Co., Crystal and Electronic Products Department, Ohio 44139.

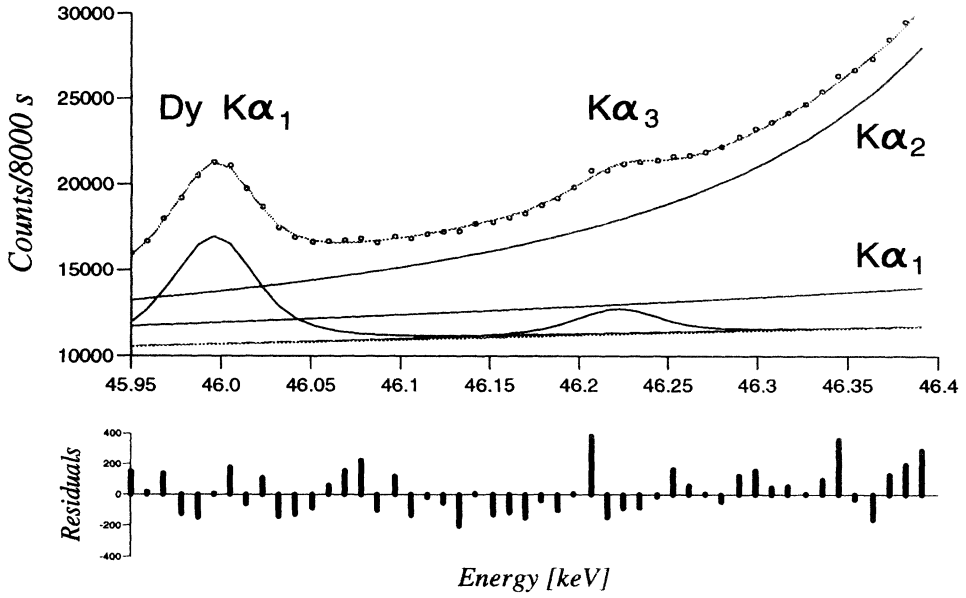

FIG. 2. Part of the $K\alpha$ x-ray spectrum of $_{67}$Ho with the $K\alpha_3$ line. The second line on the left stems from a dysprosium impurity ($_{66}$Dy $K\alpha_1$) in the target. The figure shows also the low energy tail of the $K\alpha_1$ and $K\alpha_2$ lines (solid lines) and the linear background (dotted line) as determined by the fitting procedure. Residuals, i.e., differences between measured intensities and fitted ones, are presented too.

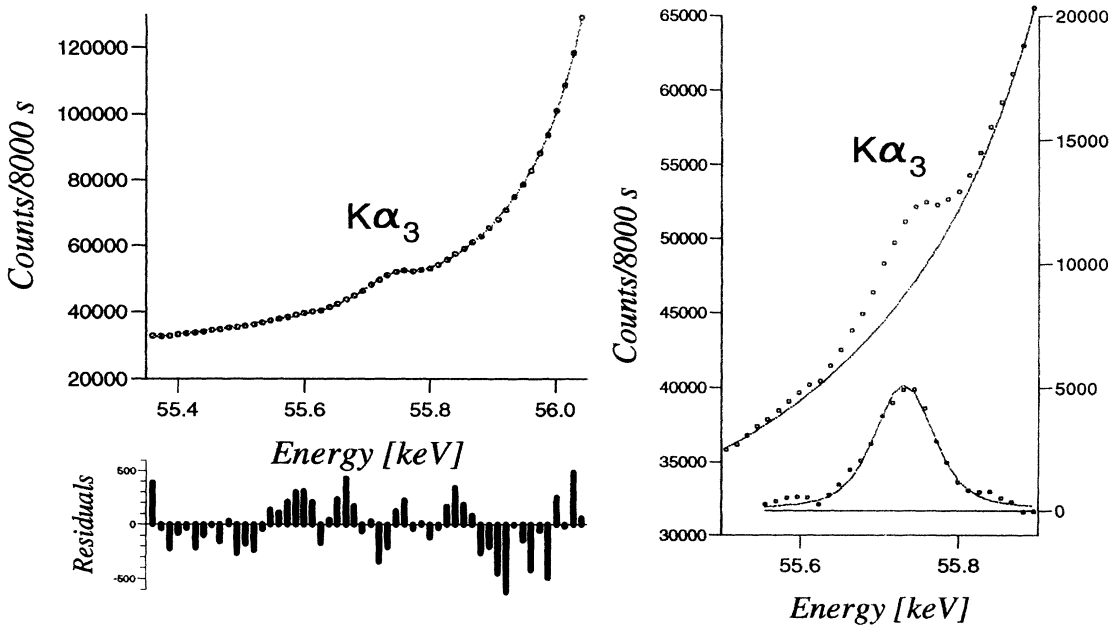

FIG. 3. Crystal spectrometer spectrum of $_{73}$Ta $K\alpha_3$ x-rays induced by photoionization. The dots correspond to the experimental points and the curves to the total fit with residuals in the left figure and to the total fit without the $K\alpha_3$ component in the right upper figure. The right lower figure shows the fitted $K\alpha_3$ line after subtraction of the background and $K\alpha_1$ and $K\alpha_2$ tails.

III. DATA ANALYSIS

A. X-ray line shape

The observed K x-ray lines were analyzed by means of a least-squares-fit computer program (package MINUIT [14], CERN Library) using Voigt profiles. The Voigt profile $V(E)$ [15] results from the convolution of the natural x-ray line shape, which is given according to Weisskopf-Wigner's theory [16] by a Lorentzian function $L(E)$, with the Gaussian instrumental response $G(E)$ of the spectrometer:

$$\begin{aligned} V(E) &= \lim_{n\to\infty}\int_{-n}^{+n} L(E-E')G(E')dE' \\ &= \lim_{n\to\infty}\int_{-n}^{+n} \frac{A}{(\frac{1}{2}\Gamma)^2+(E-E'-E_0)^2} \\ &\quad\times\exp[-(E')^2/2\sigma^2]dE', \end{aligned} \tag{2}$$

where A is the amplitude of the peak, E_0 the energy of its centroid, Γ the Lorentzian FWHM and σ the standard deviation of the Gaussian distribution. σ is related to the FWHM by FWHM$=2\sqrt{2\ln(2)}\sigma$. The function $V(E)$ was evaluated numerically by means of the complex error function method [17,18].

B. $K\alpha$ spectra

For the analysis of the $K\alpha$ spectra, the following functional was employed to fit the data:

$$F(E) = B(E) + \sum_{i=1}^{3} V_{K\alpha_i}(E) + \sum_{i=1}^{n} V_i(E), \tag{3}$$

where $B(E)$ is a linear function of energy representing the background, $V_{K\alpha_i}(E)$ are Voigt functions describing the $K\alpha$ x-rays from the target and $V_i(E)$ are Voigt functions describing the K x-rays from trace elements present in the target. Such trace element x-rays were observed, for instance, in the holmium spectrum (Fig. 2). Fortunately, most spectra were free of these parasitic x-ray lines and could therefore be analyzed without taking into consideration the last sum in (3).

In the fitting procedure, the slope of the background and its amplitude at the energy position of the $K\alpha_1$ line centroid as well as the intensities, energies, and Gaussian widths of the x-ray lines were let free. The Lorentzian widths were taken from the tables of Salem and Lee [19] and kept fixed. Since Salem and Lee's values result from a fit to experimental data, they were preferred to theoretical values as, for instance, those of Krause and Oliver [20].

C. $K\alpha_3$ transitions

In the energy region corresponding to the $K\alpha_3$ line, the main contribution to the measured intensity stemmed from the low energy tail of the $K\alpha_2$ line, some from the $K\alpha_1$ tail and from the background, whereas only a minor part originated from the forbidden $2s_{1/2}$-$1s_{1/2}$ radiative transition (Fig. 2). The analysis of the $K\alpha_3$ lines was therefore very sensitive to the $K\alpha_2$ low energy tails, the shapes of which represented the main source of uncertainty in the determination of the $K\alpha_3$ yields. In this respect, the choice of a proper crystal for the diffraction of the x rays was of prime importance. Previous measurements performed with a 2.5 mm thick crystal having a non-perfectly-symmetrical response function resulted in inconsistent values for the fitted $K\alpha_3$ yields. The latter varied by a factor of 2, depending on the parameters of the additional peaks introduced in the analysis to take into account the asymmetry of the x-ray lines. The 1 mm thick crystal used in the presented experiment had a somewhat worse resolution (9.6 arcsec instead of 7.5 arcsec for the thicker crystal), but no asymmetry was observed of the line profiles.

The $K\alpha_3$ spectra were analyzed with the same method as the one used for the $K\alpha$ spectra. However, only the energies and the intensities of the $K\alpha_3$ and $K\alpha_2$ lines were let free in the fitting procedure. All other parameters were kept fixed at the values obtained from the analysis of the $K\alpha$ spectra. In principle, the energy of the $K\alpha_2$ line could also have been kept fixed in the fitting procedure whereas the $K\alpha_2$ intensity had to be varied due to the large differences in the acquisition time of the $K\alpha$ and $K\alpha_3$ spectra. However, both parameters were let free because better fits of the $K\alpha_2$ tail resulted. In fact, it has emerged in the analysis that even for incomplete profiles the least-square-fit procedure converged rapidly provided that the Gaussian and the Lorentzian widths were kept fixed. Equal widths were set for the $K\alpha_3$ and $K\alpha_2$ lines. In a complementary analysis the Lorentzian width of the $K\alpha_3$ line was let free. No significant change in the $K\alpha_3$ intensities was observed whereas the uncertainties of the $K\alpha_3$ natural linewidths were so large that no credit could be given to the obtained values.

IV. RESULTS AND DISCUSSION

A. Theoretical predictions

Many authors have developed the approximation for relativistic calculation of atomic x-ray emission rates (see, e.g., [21,22] and references therein). In this paper we compare our experimental results with MCDF calculations and Scofield's predictions.

Relativistic multiconfiguration Dirac-Fock (MCDF) calculations were performed by Polasik in the extended average-level version (MCDF-EAL) [23] with the program package GRASP (general-purpose relativistic atomic structure program). A detailed description of the program developed by Grant and co-workers is given, for instance, in Ref. [24].

Relativistic atomic orbitals are one-electron four-component spinor eigenfunctions of angular momentum operators $\hat{j}^2$, $\hat{j}_z$, and parity $\hat{p}$. These orbitals are obtained as solutions of the Dirac-Fock equations. Config-

uration state functions (CSF's) are built from antisymmetrized products of such orbitals and have a prescribed coupling scheme, parity P, and total angular momentum J and M quantum numbers. Multiconfiguration atomic state functions are linear combinations of CFS's.

Within the MCDF scheme, the effective Hamiltonian for the N-electron system is expressed, if atomic units are used, by

$$H = \sum_{i=1}^{N} h_D(i) + \sum_{i<j}^{N} C_{ij}, \tag{4}$$

where $h_D(i)$ is the Dirac operator for ith electron and the terms C_{ij} account for electron-electron interactions and correspond to one-photon exchange processes. Each C_{ij} can be expressed [25] by $C_{ij} = 1/r_{ij} + T(r_{ij})$, where $1/r_{ij}$ is the Coulomb interaction operator (due to longitudinally polarized photons) and $T(r_{ij})$ is the transverse Breit operator (due to transversely polarized photons). Only the Coulomb repulsion of the electrons is initially included in the self-consistent-field procedure. Contributions due to retarded Coulomb interaction, the polarization of the vacuum by the nuclear charge distribution, higher-order corrections due to the transverse electromagnetic interaction (Breit), and the radiative corrections (self-energy) are taken into account as a first-order correction to the energy levels and treated via perturbation theory. In the alternative MCDF-EAL version of the calculations, the energy functional is statistically averaged over all the initial and final states.

The calculations of relativistic radiative transition probabilities have been based on both the Coulomb and Babushkin [26] gauges (see, e.g., [27] for an interesting comparison of the two gauges). The MCDF approximation for the calculation of atomic states and transition rates can be easily found in the literature (see, e.g., [28]).

Scofield [8,29] calculated the radiative decay rates for transitions filling vacancies in the K and L shells for elements ranging from $Z = 5$ to 104. For each electron transition emission rates of all the allowed multipoles of the radiation field were calculated. In such calculations, the electrons in the initial and final states are treated as moving independently in the same central potential which is given by the neutral atom occupations of the subshells. The effect of retardation is included. Regarding computing, a correct calculation of the exchange terms is time consuming. In the Slater approximation, these terms are replaced by a local central potential. An iterative procedure is then used to find the self-consistent potential arising from the occupation of the single-particle levels. The electrons are assumed to be in the single-particle states and are treated relativistically by using Dirac-Hartree-Slater (DHS) equations to determine the wave functions.

In Scofield's calculations, nuclear charge distributions of finite extent were taken into account but not Breit, self-energy and vacuum polarization corrections. The relativistic effects and the effect of the finite x-ray wavelength led to important corrections that were larger than 5% for K-shell transitions in heavy elements ($Z > 50$). The Babushkin gauge was used in this model. The non-vanishing $K\alpha_3$ transition rates are due to retardation and relativistic effects.

TABLE I. Comparison of the $K\alpha_3$ energies obtained from our measurements with the values given by Siegbahn [30] and Bearden [31].

Element	$K\alpha_3$ energy (eV)		
	Our experiment	Siegbahn	Bearden
$_{54}$Xe	29116 ± 2	29 113	29 108.6
$_{59}$Pr	35 156 ± 1	35 156	35 155.8
$_{64}$Gd	41 864 ± 3	41 864	41 863.5
$_{67}$Ho	46 221 ± 4	46 223	46 223.5
$_{73}$Ta	55 733 ± 2	55 733	55 734.9
$_{79}$Au	66 374 ± 7	66 369	66 372.1

B. Experimental results

The energies of the $K\alpha_3$ x-ray lines observed in our experiment are given in Table I. They are compared to values deduced from the binding energies given by Siegbahn and Karlsson [30] and to Bearden and Burr standard experimental energies [31]. The quoted uncertainties are purely statistical and correspond to a confidence level of 70%. The quality of the fits may be judged via the uniformity of the residues, as shown, for instance, in Figs. 2 and 3. A good agreement is obtained except for xenon. Although the 3 eV difference with the theoretical value of Siegbahn is hardly significant, the experimental uncertainty being 2 eV (within confidence level of 70%), the discrepancy with the energy given by Bearden is larger than 7 eV. It should be noted, however, that most of the xenon data from Bearden's compilation are empirical interpolations from semi-Moseley diagrams anchored by nearby data from solid targets. Furthermore, precise and careful measurements of K and L x-rays of xenon were performed recently by Mooney *et al.* [32]. In this work the energies of forbidden transitions, such as $2s_{1/2}$-$1s_{1/2}$, were determined from redundant combinations of K and L series measurements. For the $K\alpha_3$ line, the quoted energy is 29 112.44(24) eV. Our result is thus consistent with this accurate value within a confidence level of 92%.

The $I(K\alpha_2)/I(K\alpha_1)$ and $I(K\alpha_3)/I(K\alpha_1)$ intensity ratios extracted from our measurements are listed in Ta-

TABLE II. Comparison of our experimental $I(K\alpha_2)/I(K\alpha_1)$ intensity ratios with theoretical predictions based on Scofield's [8] and MCDF [9] calculations.

Element	Ratio $\frac{I(K\alpha_2)}{I(K\alpha_1)}$		
	Experimental (present work)	Theoretical	
		Scofield Babushkin gauge	Polasik Coulomb gauge
$_{54}$Xe	0.582 ± 0.004	0.540	0.555
$_{59}$Pr	0.554 ± 0.001	0.548	0.557
$_{64}$Gd	0.559 ± 0.004	0.556	0.571
$_{67}$Ho	0.561 ± 0.007	0.562	0.585
$_{73}$Ta	0.573 ± 0.002	0.574	0.612
$_{79}$Au	0.58 ± 0.01	0.588	0.651

TABLE III. Comparison of our experimental $I(K\alpha_3)/I(K\alpha_1)$ intensity ratios with Scofield's [8] and MCDF [9] predictions.

Element	Ratio $\frac{I(K\alpha_3)}{I(K\alpha_1)}$			
	Experimental (present work)	Theoretical		
		Scofield	Polasik	
		Babushkin gauge	Coulomb Gauge	Babushkin gauge
$_{54}$Xe	$(0.51 \pm 0.07) \times 10^{-4}$	0.547×10^{-4}	0.545×10^{-4}	0.533×10^{-4}
$_{59}$Pr	$(0.59 \pm 0.03) \times 10^{-4}$	0.984×10^{-4}	0.985×10^{-4}	0.961×10^{-4}
$_{64}$Gd	$(1.5 \pm 0.1) \times 10^{-4}$	1.701×10^{-4}	1.714×10^{-4}	1.665×10^{-4}
$_{67}$Ho	$(2.4 \pm 0.2) \times 10^{-4}$	2.326×10^{-4}	2.373×10^{-4}	2.279×10^{-4}
$_{73}$Ta	$(5.3 \pm 0.2) \times 10^{-4}$	4.22×10^{-4}	4.372×10^{-4}	4.146×10^{-4}
$_{79}$Au	$(8.3 \pm 0.5) \times 10^{-4}$	7.42×10^{-4}	7.909×10^{-4}	7.305×10^{-4}

bles II and III, respectively. Corrections were made to account for the self-absorption in the target of the observed x rays and for the intensity attenuation by the crystal thickness. In the self-absorption calculations the spectral intensity distribution of the ionizing radiation which was determined in a separate experiment was taken into account. On the other hand, corrections concerning the dependence on the energy of the crystal reflectivity were estimated to be smaller than 1% and therefore not considered. The obtained intensity ratios are compared in Tables II and III with Scofield's Hartree-Fock-Slater and Polasik's MCDF predictions. No MCDF values using Babushkin gauge are mentioned in Table II because Scofield's and MCDF calculations adopting the same gauge are identical.

From Table II one can conclude that the Coulomb gauge gives less reliable results for the $I(K\alpha_2)/I(K\alpha_1)$ intensity ratios for atomic numbers larger than about 70. A review of available experimental $I(K\alpha_2)/I(K\alpha_1)$ ratios was published by Salem *et al.* [33], who worked out least-squares fits of all data at hand for even Z. A very good agreement was found with Scofield's calculations employing the Babushkin gauge. A comparison of our experimental ratios with those of Scofield evinces also a good agreement except for xenon.

As can be seen in Table III, $I(K\alpha_3)/I(K\alpha_1)$ yield ratios of the present work seem in general to favor MCDF calculations and confirm the increase in intensity with increasing Z. It is noticeable that the result for $_{67}$Ho is in very good agreement with theoretical predictions. On the other hand, it is rather surprising that the largest difference with respect to theory is observed for praseodymium which has the smallest experimental uncertainty. With the exception of praseodymium and tantalum, our results are consistent with theory within the experimental uncertainties for metallic targets as well as for the noble gas one (Fig. 4). The discrepancies observed for Pr and Ta, therefore, cannot be explained by solid state effects. In fact, such effects are not expected for $K\alpha$ transitions of heavy elements because the shells involved in those transitions are far away from the Fermi level. In the case of xenon, for which the $K\alpha_3$ intensity is very weak, a complementary analysis was performed with the $K\alpha_3$ energy kept fixed in the fitting procedure at the above mentioned value from Mooney *et al.* The obtained $I(K\alpha_3)/I(K\alpha_1)$ yield ratio was $(0.50 \pm 0.04) \times 10^{-4}$, a value which is quite consistent with the result given by the first analysis (Table III).

As a retrospect, Fig. 5 presents our results and the previous experimental information on $I(K\alpha_3)/I(K\alpha_1)$ ratios. This picture shows some discrepancies between experimental data from different sources. Our results do

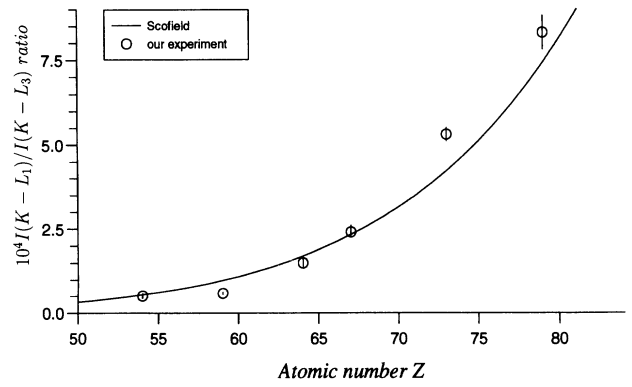

FIG. 4. Experimental ratios of the $K\alpha_3$ ($M1$ transition) to the $K\alpha_1$ ($E1$ transition) rates. The theoretical curve was generated from the numerical data taken from Ref. [8]. Numerical experimental values are printed in Table III.

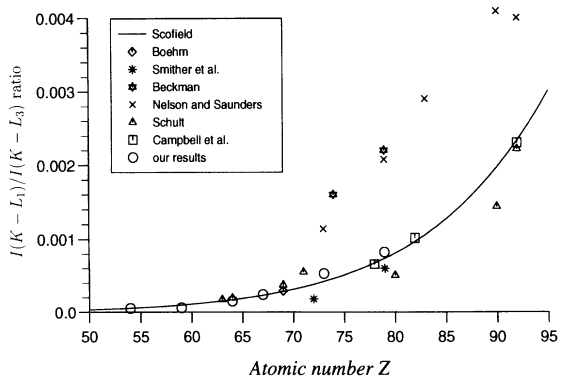

FIG. 5. Ratio of the $K\alpha_3$ ($M1$ transition) to the $K\alpha_1$ rates versus Z. Present and previous measurements [1–7], compared with Scofield's DHS calculations [8].

not confirm that Scofield's predictions are too low, as anticipated from some previous data.

V. CONCLUSION

Our study provides experimental support for theoretical $K\alpha$ x-rays relative intensity ratios. In particular, on the basis of the present measurements with a high resolution crystal spectrometer, it has been shown that, the experimental $I(K\alpha_3)/I(K\alpha_1)$ ratios are in good agreement with the theoretical predictions. No systematic deviation in function of Z has been observed.

ACKNOWLEDGMENTS

The authors are indebted to Dr. Marek Polasik for performing calculations with the code GRASP. This work was partly supported by the Swiss National Science Foundation.

[1] O. Beckman, Ark. Fys. **9**, 495 (1955).
[2] R. K. Smither, M. S. Freedman, and F. T. Porter, Phys. Lett. A **32**, 405 (1970).
[3] F. Boehm, Phys. Lett. A **33**, 417 (1970).
[4] O. W. B. Schult, Z. Naturforsch. Teil A **26**, 368 (1970).
[5] G. C. Nelson and B. G. Saunders, J. Phys. (Paris) Colloq. **32**, C4-97 (1971).
[6] J. L. Campbell and C. W. Schulte, Phys. Rev. A **22**, 609 (1980).
[7] J. L. Campbell *et al.*, Phys. Rev. A **33**, 986 (1986).
[8] J. H. Scofield, At. Data Nucl. Data Tables **14**, 121 (1974).
[9] M. Polasik (private communication).
[10] B. Perny *et al.*, Nucl. Instrum. Methods Phys. Res. Sect. A **267**, 120 (1988).
[11] J. Hoszowska, J.-Cl. Dousse, and Ch. Rhême, Phys. Rev. A **50**, 123 (1994).
[12] W. Schwitz, Nucl. Instrum. Methods **154**, 95 (1978).
[13] R. C. Sharma *et al.*, Nucl. Instrum. Methods **130**, 305 (1975).
[14] F. James and M. Roos, Comput. Phys. Commun. **10**, 343 (1975).
[15] B. L. Roberts, R. A. J. Riddle, and G. T. A. Squier, Nucl. Instrum. Methods **130**, 559 (1975).
[16] V. Weisskopf and E. Wigner, Z. Phys. **63**, 54 (1930).
[17] C. J. Batty, S.D. Hoath, and B. L. Roberts, Nucl. Instrum. Methods **137**, 179 (1976).
[18] K. S. Kölbig, Commun. ACM **15**, 465 (1972).
[19] S. I. Salem and P. L. Lee, At. Data Nucl. Data Tables **18**, 233 (1976).
[20] M. O. Krause and J. H. Oliver, J. Phys. Chem. Ref. Data **8**, 329 (1979).
[21] R. J. S. Crossley, Adv. At. Mol. Phys. **5**, 237 (1969).
[22] I. P. Grant and H. M. Quiney, Adv. At. Mol. Phys. **23**, 37 (1987).
[23] M. Polasik, Phys. Rev. A **40**, 4361 (1989).
[24] K. G. Dyall *et al.*, Comput. Phys. Commun. **55**, 425 (1989).
[25] J. Hata and I. P. Grant, J. Phys. B **16**, 3713 (1983).
[26] F. A. Babushkin, Acta Phys. Pol. **25**, 749 (1964).
[27] I. P. Grant, J. Phys. B **7**, 1458 (1974).
[28] I. P. Grant, *Relativistic Effects in Atoms and Molecules* in *Methods in Computational Chemistry*, edited by S. Wilson (Plenum, New York, 1988), Vol. 2.
[29] J. H. Scofield, Phys. Rev. **179**, 9 (1969).
[30] H. Siegbahn and L. Karlsson, *Encyclopedia of Physics*, edited by S. Flügge (Springer-Verlag, Berlin, 1957), Vol. 31.
[31] J. A. Bearden and A. F. Burr, Rev. Mod. Phys. **39**, 125 (1967).
[32] T. Mooney *et al.*, Phys. Rev. A **45**, 1531 (1992).
[33] S. I. Salem, S. L. Panossian, and A. Krause, At. Data Nucl. Data Tables **14**, 92 (1974).